NANOSYSTEMS:
PHYSICS, CHEMISTRY, MATHEMATICS

Luginina A.A., et al. *Nanosystems: Phys. Chem. Math.*, 2022, **13** (6), 698–708.
http://nanojournal.ifmo.ru
DOI 10.17586/2220-8054-2022-13-6-698-708

Original article

High lignin content cellulose nanofibrils obtained from thermomechanical pulp

Anna A. Luginina[1,a], Sergey V. Kuznetsov[1,b], Alexander A. Alexandrov[1,c], Radmir V. Gainutdinov[2,d], Dmitrii I. Petukhov[3,e], Valery V. Voronov[1,f], Elena V. Chernova[1,g], Pavel P. Fedorov[1,h]

[1]Prokhorov General Physics Institute of the Russian Academy of Sciences, Moscow, Russia
[2]Shubnikov Institute of Crystallography of Federal Scientific Research Centre Crystallography and Photonics of Russian Academy of Sciences, Moscow, Russia
[3]Lomonosov Moscow State University, Chemical department, Moscow, Russia

[a]ana@lst.gpi.ru, [b]kouznetzovsv@gmail.com, [c]alexandrov1996@yandex.ru, [d]rgaynutdinov@gmail.com, [e]di.petukhov@gmail.com, [f]voronov@lst.gpi.ru, [g]e-chernova@yandex.ru, [h]ppfedorov@yandex.ru

Corresponding author: P. P. Fedorov, ppfedorov@yandex.ru

ABSTRACT High-lignin content cellulose nanofibrils (LCNF) were successfully prepared from thermomechanical pulp through TEMPO-catalyzed oxidation, followed by ultrasonic treatment. Preparation protocols of the LCNFs included use of the mild pre-hydrolysis of the thermomechanical pulp and adjustment of sodium hypochlorite loading for the samples with the 23.8 and 14.1 wt.% lignin content, resulting in the increase of the carboxyl group content from 0.70 to 1.24 mmol/g. LCNFs had a diameter of 14 ± 5 nm (AFM evaluation); and the LCNF morphology was affected by contents of both lignin and carboxyl groups. The translucent LCNF films were prepared by solution casting technique. They exhibited the heightened water contact angle of 75–82°, an increased thermal stability up to 275°C compared to lignin-free cellulose nanofibril films (39° and 203°C, respectively), and excellent UV-blocking ability in a wide spectrum range from 200 to 375 nm. The said LCNFs can be successfully used for manufacturing the packaging materials and/or making the biopolymer composites.

KEYWORDS cellulose, lignin, nanofibrils, nanocomposites, UV-blocking ability.

ACKNOWLEDGEMENTS This work was supported by the Ministry of Science and Higher Education within the State assignment to Prokhorov General Physics Institute of the Russian Academy of Sciences. The TG measurements were supported by the equipment of the Collective Use Center of the Prokhorov General Physics Institute of the Russian Academy of Sciences. We thank Volga Corporation for providing thermomechanical pulp sample. Authors express their sincere gratitude to Dr. Arthur I. Popov for his most kind assistance in the preparation of the present manuscript and Mr. Ilya Tronev for conductometric titration measurements.

FOR CITATION Luginina A.A., Kuznetsov S.V., Alexandrov A.A., Gainutdinov R.V., Petukhov D.I., Voronov V.V., Chernova E.V., Fedorov P.P. High lignin content cellulose nanofibrils obtained from thermomechanical pulp. *Nanosystems: Phys. Chem. Math.*, 2022, **13** (6), 698–708.

1. Introduction

Cellulose nanofibrils (CNF), obtained from various cellulose sources, attracted attention of modern researchers as "green alternative" for plastics used in polymer composites, packaging materials, optoelectronic and electronic materials, detectors, medicine and healthcare, etc. [1–10]. For the first time, CNFs were obtained by mechanical fibrillation of cellulose fibers in high-pressure homogenizer in 1983 [11, 12]. In subsequent years, researchers focused their attention at manufacturing completely bleached lignin-free CNFs by various cellulose fibrillation techniques such as microfluidization, grinding/refining, milling, cryo-crushing, steam explosion, and ultrasonication [13, 14]. Recently, a new strategy of direct conversion of lignocellulose into nanofibrils was suggested; and it resulted in the preparation of so-called lignin-containing nanofibrils (LCNF) [15–20]. Also, the said recent publications [16–18] disclose preparation of LCNF from various lignocellulose sources including wood species, plant-based biomass, unbleached kraft pulp, etc. Making LCNF is more efficient and ecologically friendly compared to CNF manufacturing because of the use of non-delignified raw material, requires less energy and smaller amounts of chemical reagents; it also allows more rational and complete use of renewable resources.

Lignin is an amorphous aromatic copolymer; it is a major incrusting ingredient of the plant cell walls: the latter are made up of endurable cellulose nanofibrils that are built in the lignin-hemicellulose matrices [21]. Lignin is more hydrophobic than cellulose; it possesses UV-protecting, antibacterial and antioxidant properties [22, 23]. As a result, lignin is used as green reinforcing component of CNF UV-protecting films [24–26].

Composite nano-lignin CNF films have exhibited antibacterial activity against Escherichia coli and hemolytic streptococci [26]. Authors [27–29] emphasized that lignin improved hydrophobicity of LCNFs compared to the one of CNFs. As a result, enhanced LCNF hydrophobicity allowed use of the said materials as ingredients of hydrophobic matrix composites [30–33].

Thus, the thermomechanical pulp (TMP) with high content of lignin can become an important starting material for making LCNF in order to provide the manufactured materials with the hydrophobic, UV-protecting and/or antibacterial properties. However, the presence of lignin lowers efficiency of cellulose fibrillation under mechanical treatment [20]. The said fibrillation efficiency can be improved by preliminary enzymatic or chemical treatment like 2,2,6,6-tetramethylpiperidine-1-oxyl radical (TEMPO) mediated oxidation, which is used quite frequently because of the high homogeneity of obtained CNFs. Such TEMPO-catalyzed oxidation of cellulose was originally implemented by Isogai and Kato in 1998 [34], and it was optimized later by Isogai and Saito [35, 36] for making CNFs from cotton and bleached pulp.

In view of the above said, the goals of our present study were preparation of lignin containing cellulose nanofibrils from thermomechanical pulp of spruce and making hydrophobic films with UV blocking effect based on the said nanofibrils.

2. Experimental methods

2.1. Materials

As the starting materials, we used 15 wt.% spruce thermomechanical pulp (TMP) (Volga company, Balakhna, Nizhny Novgorod region, Russia), powdered bleached woodkraft cellulose (PCC-0.25) (Polycell, Vladimir, Russia), 99% pure TEMPO (NIOCH SB RAS, Russia) 19 wt.% sodium hypochlorite solution; sodium bromide; sodium hydroxide; and hydrochloric acid (analytical grade) (all four reagents were supplied by Chimmed, Russia).

2.2. TMP pre-treatments

The TMP samples were squeezed out on a nylon mesh and dried under air for the further storage and use. Before their use, TMP specimens were ground in the laboratory mill LZM-1M with the rotary knife. Shredded TMP fibers (2.0 wt.%) were swollen in double distilled water at room temperature for 12 h, then refrigerated below 5°C for 30 days. The resulting samples were labeled as TMP_{pr}.

2.3. Control samples

Lignin-free TEMPO-oxidized cellulose nanofibrils (TOCNF) samples were prepared from PCC-0.25 powdered wood bleached kraft cellulose according to the previously published technique [37] and served as control specimens.

2.4. TEMPO-mediated oxidation of TMP

TEMPO-mediated oxidation of TMP was carried out by modified [8, 37] techniques (see protocols 1 and 2 below).

2.4.1. Protocol 1. 100 ml of 11.5 M HCl was slowly added under stirring to prepared as described above 500 g of lignocellulose fiber TMP_{pr} (2.0 wt.%). Obtained ∼2 M HCl solution was placed in the 80°C water bath and hydrolyzed under vigorous stirring for 30 min. The reaction was quenched by 10-fold dilution with cold double distilled water. Then, the obtained suspension was washed with double distilled water, using repeated centrifugation cycles, until pH 5.0 was reached. The content of hydrolyzed lignocellulose fiber was determined gravimetrically. 400 ml of aqueous solution of 0.1600 g TEMPO and 1.0000 g NaBr was added to the resulting suspension of 10 g of hydrolyzed lignocellulosic fiber in 600 ml of water, and the formed mixture was stirred for 10 minutes. Oxidation was initiated by slow dropwise addition of 11.9 wt.% NaClO solution (5 mmol/g TMP) with constant stirring at room temperature. The pH of the suspension was maintained at 10.2–10.5 and, if necessary, adjusted by adding 0.3 M NaOH. The oxidation reaction was completed and the suspension pH levelled off in about 50 min. Then, pH was further adjusted to about 7.0 by adding 0.5 M HCl. The supernatant was separated from the precipitate, the latter was suspended in H_2O and centrifuged at 8000 rpm for 10 minutes. The centrifuged precipitate was redispersed in double distilled water, ultrasonicated in the ice bath at 35 kHz frequency for 30 minutes, and subjected to dialysis against water for 7 days. After dialysis, the suspension was once again ultrasonicated in an ice bath for 30 minutes. The resulting lignin-containing cellulose nanofibrils samples were labeled as $LCNF_1$ and stored at 4°C. The LCNF content in the $LCNF_1$ dispersion was determined gravimetrically.

2.4.2. Protocol 2. 500 g of lignocellulosic fiber TMP_{pr} sample (2.0 wt.%), prepared as described above, was treated with 500 ml aqueous solution containing 0.1600 g TEMPO and 1.0000 g NaBr under stirring for 10 minutes. The oxidation was initiated by the slow addition of 11.9 wt.% aqueous NaClO to 10 mmol/g TMP under constant stirring at room temperature. The pH of the suspension was maintained at 10.2–10.5 and, if necessary, adjusted by adding 0.3 M NaOH. After 65 min, the oxidation reaction was completed, pH of the suspension stopped changing, and the reaction mixture pH was adjusted to about 7.0 by adding 0.5 M HCl. The further work-up procedure was similar to the one described above in the protocol 1. The resulting lignin-containing cellulose nanofibrils samples were labeled as $LCNF_2$ and stored at 4°C. The LCNF content in the $LCNF_2$ dispersion was determined gravimetrically.

2.5. Fabrication of lignin containing cellulose nanofibrils films

Suspensions of $LCNF_1$ or $LCNF_2$ were diluted with double distilled water to the 1.0–2.2 wt.% solids content. 10 ml specimens of the obtained suspensions were ultrasonicated in an ice bath for 5 minutes (UZG13-01/22 sonicator, 110 W, VNIITVCH), poured into polystyrene Petri dishes (35 mm diameter), and dried under ambient conditions for 3–4 days. After evaporation of the solvent, the formed $LCNF_1$ and $LCNF_2$ films were carefully separated from the plastic substrates as a self-standing structure. Subsequent drying of the films was carried out at 70°C for 40 min.

2.6. Characterization

X-ray diffraction analysis of the samples was carried out on a Bruker D8 Advance diffractometer (Bruker AXS GmbH, Karlsruhe, Germany) on CuKα-radiation in the angular range 8–60 °2θ, in steps of 0.02 °2θ. The diffraction peak about 22.7 2Θ was used for TOCNF crystallinity index (IC, %) calculation by Segal's method [4].

Conductometric titration was used to determine carboxyl groups content in mmol/g of LCNF according to the protocol described elsewhere [38]. The conductivity values were recorded using conductometer Expert-002 at room temperature as the mean value of three measurements.

The surface morphology and roughness were investigated using a NTEGRA Prima atomic force microscope (NTMDT Spectrum Instruments, Russia) in tapping mode. All experiments were carried out under controlled conditions maintained by a TRACKPORE ROOM-05 measuring complex (purity class 5 ISO (100), the accuracy of maintaining air temperature in the range 23 ± 5 K is ± 0.05 K, the relative air humidity is 55 ± 1 %). The average roughness (Ra) was measured from the AFM image for 10 μm $\times$ 10 μm scanning area.

Thermogravimetric analysis (TG) was performed in 23–650°C range with 5°C/min heating rate in a synthetic air flow (50 ml/min) and an argon flow (20 ml/min) using a STA 449F3 Jupiter calorimeter with a TG sensor (Netzsch, Germany). The weight part was preliminarily calibrated by the decomposition of a standard reagent, calcium oxalate hydrate $CaC_2O_4 \cdot xH_2O$.

Fourier transform infrared spectroscopy (FTIR) was performed on an INFRALUM FT-08 spectrometer with ATR unit (Pike) from 400 to 4000 cm^{-1}.

The transmission spectra were recorded using a Cary 5000 spectrophotometer in the 200–800 nm range.

The contact angle was measured on a FTA1000 Drop Shape Instrument B Frame System. The test sample was placed on a horizontal holder. The water was applied onto the surface of the test sample by a special microdosing syringe. The droplet volume was 100 μl. The images were recorded using a CCD detector of 640·480 pixels. Images were obtained after 1 s application of the droplets. The measurements were performed at room temperature (24 ± 2°C) and repeated 5 times on various fresh surfaces.

The chemical composition of dried up at 105 °C samples TMP and LCNF was determined in accordance with the standards of the Technical Association of the Pulp and Paper Industry (TAPPI). The holocellulose (alfa-cellullose + hemicelluloses) content was determined according to the method described in TAPPI 249-75. The alpha-cellulose content was then determined by T203-99. The difference between the values of holocellulose and alfa-cellulose content gives the hemicellulose content [39]. The lignin in lignocellulosic fiber (TMP, $LCNF_1$ and $LCNF_2$) includes acid-insoluble lignin and acid-soluble lignin. Acid-insoluble lignin content was analyzed by reaction with 72% H_2SO_4, using a standard method recommended in TAPPI T222 om-88. The acid-soluble lignin content was determined in the filtrate after the separation of acid-insoluble lignin by the spectrophotometric method at a wavelength of 240 nm [40]. Each sample was tested three times, and the averaged values were obtained.

3. Results and discussion

3.1. Preparation of LCNF with different lignin contents

The chemical composition of the original lignocellulosic raw material was compared with the composition of obtained LCNF. Thermomechanical pulping is the process of producing wood pulp at elevated temperature and pressure in refiners from pre-steamed wood chips at a temperature of about 125 °C. With such thermo-hydrolytic treatment, some of the organic substances contained in wood can dissolve in water [41]. The chemical composition of samples on dry weight and yields of LCNF from each protocol are shown in Table 1. It can be seen from the data that the cellulose content and the total content of the main components in TMP_{pr} slightly increased compared to wood chips, by 2.8% and 2.0%, respectively, which indicates the removal of extractives, including terpenes, resin and fatty acids.

The results showed that the $LCNF_1$ yield was slightly (1%) higher than the $LCNF_2$ yield. LCNF yield from native wood was about 2 times higher than TOCNF, Table 1. During TEMPO oxidation, the content of α-cellullose in TOCNF increased, the content of hemicelluloses decreased, and lignin was absent. Previously, it was shown that selective oxidation of the primary hydroxyl groups of cellulose occurs, as well as the decomposition of hemicelluloses and the oxidation of lignin during TEMPO oxidation [35, 36]. The content of lignin decreased in both protocols when using TMP_{pr}, much decreased by twice in protocol 2 when using higher doses of NaClO. The increase in oxidation in the case of $LCNF_2$ is confirmed by a higher carboxyl group content of 1.24 mmol/g compared to 0.70 mmol/g in $LCNF_1$, Table 1. The amount of lignin decreased by Protocol 1 compared to TMP_{pr} by 4.7%, however, the amount of lignin in $LCNF_1$ (23.8%)

TABLE 1. Chemical composition of samples on dry weight and yields of LCNF from each protocol

Sample	α-cellullose, wt.%	Hemicellu-loses, wt.%	Lignin, wt.%			Yield, (%)		Carboxyl group content (C_{cg}), mmol/g
			total	acid-insoluble	acid-soluble	process output	from native wood	
spruce wood[42]	42	25	29			–		–
TMP_{pr}	44.8 ± 0.5	24.7 ± 0.2	28.5 ± 0.3	27.7	0.8	–	94[41]	–
$LCNF_1$	68.4 ± 0.5	5.7 ± 0.2	23.8 ± 0.3	23.1 ± 0.3	0.7 ± 0.2	65	61	0.70 ± 0.05
$LCNF_2$	69.5 ± 0.5	14.3 ± 0.2	14.1 ± 0.3	11.3 ± 0.3	2.8 ± 0.2	64	60	1.24 ± 0.05
TOCNF[8]	96.0 ± 0.5	3.4 ± 0.2	0	0	–	70	30	1.12 ± 0.05
PCC-0.25[8]	92.9 ± 0.4	5.2 ± 0.2	1.2 ± 0.3	1.2 ± 0.3	–	–	43[43]	–

is much higher than in other studies [16, 17, 42]. With a decrease of acid-insoluble lignin content in $LCNF_2$, increased of acid-soluble lignin content 2.1% compared to $LCNF_1$. During TEMPO oxidation of TMP_{pr} using higher doses of NaClO (10 mmol/g), part of the lignin decomposed, part of the lignin was oxidized to form fragments with a lower molecular weight of acid-soluble lignin. A similar effect was observed during TEMPO oxidation of poplar alkaline peroxide mechanical pulp [44]. According to protocol 1, a preliminary mild hydrolysis of TMP_{pr} with dilute HCl was performed, followed by TEMPO oxidation. During mild hydrolysis of TMP_{pr} with dilute acid, first of all, amorphous hemicelluloses are hydrolyzed, then partially amorphous regions of cellulose, lignin is not dissolved, but some structural changes of lignin can occur during this treatment [22, 41]. The significantly lower hemicellulose content in $LCNF_1$ compared to $LCNF_2$ is due to the mild hydrolysis step of Protocol 1 (Table 1). The appearance of the TMP_{pr} suspension changed during the oxidation of TEMPO (Fig. 1). The original yellow-light brown TMP_{pr} pulp was a suspension of swollen lignocellulose fibers in water with phase separation, Fig. 1a. The gel-like suspension on protocol 1 turned brown while the $LCNF_2$ gel-like suspension remained yellow, Figs. 1b and c. The change in the color of the $LCNF_1$ pulp to dark brown may be associated with an increase in chromophore groups in the lignin structure after treatment with dilute HCl.

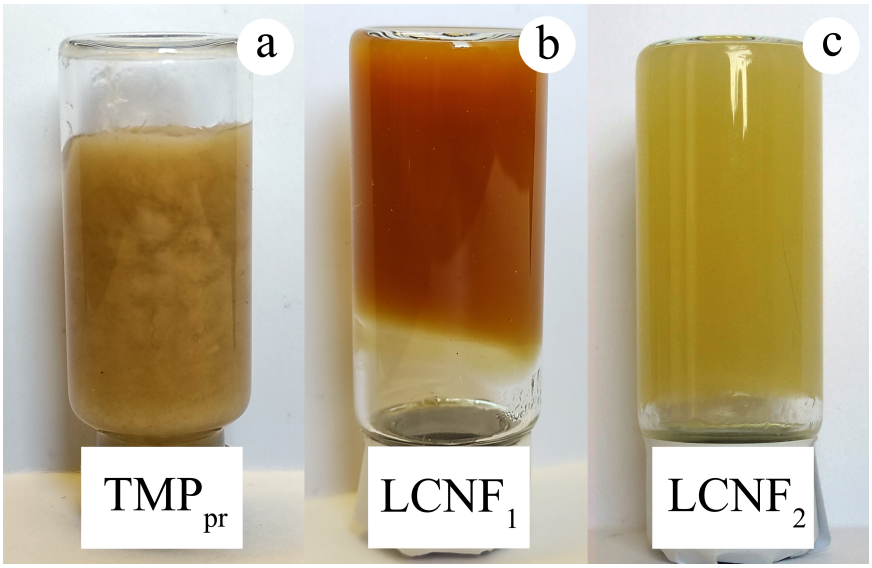

FIG. 1. Appearance of aqueous suspensions: (a) TMP_{pr} (2.5 wt.%); (b) $LCNF_1$ (2.5 wt%), (c) $LCNF_2$ (2.5 wt%)

X-ray diffraction patterns of all samples contained diffraction peaks at $2\theta = 22.3^\circ$ and $2\theta = 14.8 - 16.8^\circ$ (double peak) that corresponded to the (200), $(1\bar{1}0)$ and (110) crystallographic planes of monoclinic Iβ cellulose [38] (Fig. 2). Obviously, the crystal structure of the samples treated according to Protocol 1 and 2 did not change and remained cellulose I. However, the crystallinity index (IC) varied significantly under different processing conditions. The high IC = 78.2% for the TOCNF sample was due to its high content of α-cellulose, low content of amorphous hemicelluloses, and the absence of lignin. The IC value for $LCNF_1$ and $LCNF_2$ was 62.5% and 64.7%, respectively. This was consistent with the

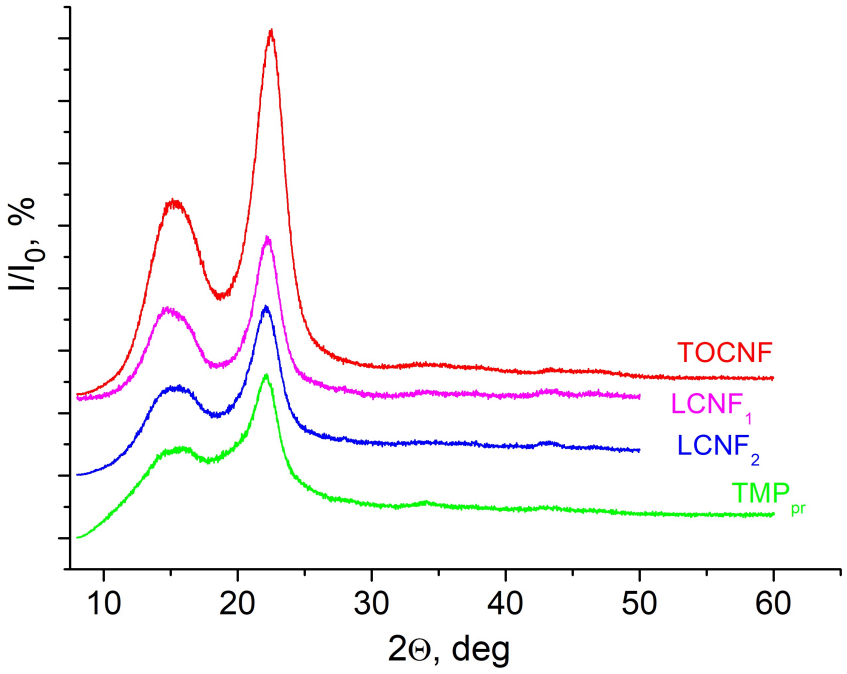

FIG. 2. XRD patterns of the TMP_{pr} and films: $LCNF_1$, $LCNF_2$, TOCNF

TABLE 2. Physical properties of TOCNF, $LCNF_1$, $LCNF_2$ films

Sample	Particle size, nm		Crystallinity index (IC), %	Average roughness (Ra), nm	WCA, deg. (°)
	fibril diameter	sphere diameter			
$LCNF_1$	14 ± 5	14 ± 8	62.5	61	75 ± 2
$LCNF_2$	14 ± 5	10 ± 3	64.7	37	82 ± 2
TOCNF[8]	19 ± 5	–	78.2	3	39 ± 3

results of the content of α-cellulose in them (Table 1). An increase in the intensity of the amorphous halo and lower value IC (53.3%) for TMP_{pr} was associated with a high content of hemicelluloses and lignin.

3.2. Characterization of chemical structures and morphology of $LCNF_1$, $LCNF_2$ films

FTIR was carried out to characterize the chemical structure of LCNF with different lignin content (Fig. 3). FTIR spectra of all samples comprise absorption bands typical for cellulose: 3284–3344 cm^{-1}, 2899 and 1644 cm^{-1} have been assigned to the stretching vibration of O–H hydrogen bond, C–H stretching, respectively. The 1644 cm^{-1} band is associated with OH bending of the absorbed water vibrations. Three bands at 1422 cm^{-1}, 1367 cm^{-1} and 1315 cm^{-1} are associated with cellulose parent chain. 1158 cm^{-1} band corresponds to the asymmetric bridge C–O–C stretching. 1104 cm^{-1} and 1026 cm^{-1} bands are associated with C–O–C pyranose ring skeletal vibrations. A small sharp band at 898 cm^{-1} is attributed to the β-glycosidic linkages between the anhydroglucose rings in the cellulose [39].

For all samples at 1607 cm^{-1} the absorption band associated with the C=O stretching vibration of the carboxylate groups the formed as a result of the TEMPO-mediated oxidation reaction can be observed [38]. The intensity of the band at 1607 cm^{-1} is maximum for $LCNF_2$ (C_{cg} = 1.24), decreases with a decrease carboxyl group content for TOCNF (C_{cg} = 1.12) is minimal for $LCNF_1$ (C_{cg} = 0.70).

Bands at 1509 cm^{-1} and 1262 cm^{-1} are attributed to C = C stretching vibration in the aromatic ring and the C–O stretching from lignin, respectively [45–47], are visible for $LCNF_1$ and $LCNF_2$ samples as shown in Fig. 5. With the decrease of lignin content (Table 1), the characteristic bands of lignin in $LCNF_2$ samples weakened and disappear in lignin-free TOCNF. Additional absorption band in FTIR spectrum for $LCNF_1$ at 1705–1740 cm^{-1} is attributed to carbonyls group and the ester linkage of carboxylic group of the ferulic and p-coumaric acids of lignin [22, 48], which is due to the preliminary hydrolysis of dilute HCl according to protocol 1. The absence of this band in the $LCNF_2$ spectrum confirms the assumption made.

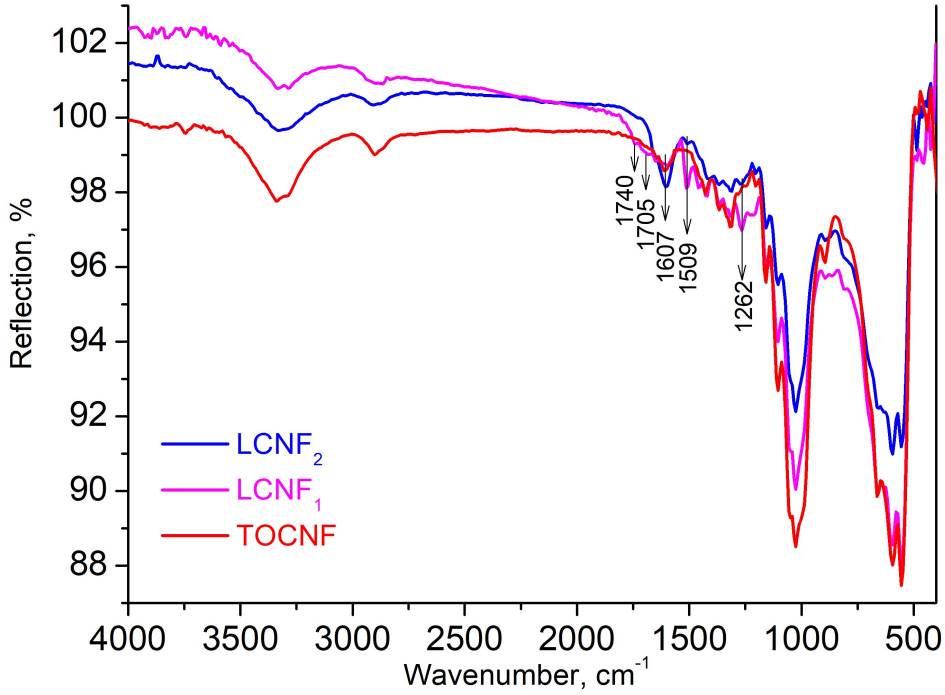

FIG. 3. FTIR spectra of: TOCNF, $LCNF_1$, $LCNF_2$

The morphology of LCNF and TOCNF films studied using AFM is shown in Fig. 3. The microstructure of TMP_{pr} fibers is shown in Fig. 1S. The diameter and length of the TMP_{pr} fiber were 30 ± 10 μm and 750 ± 250 μm, respectively.

The TOCNF samples contained entangled nanofibrils 19 ± 5 nm diameter (Fig. 4a). Cellulose nanofibrils as well as dispersed spherical nanoparticles were observed in $LCNF_1$ and $LCNF_2$ samples (Figs. 4b and 4c). The spherical nanoparticles most likely consisted of lignin. Similar structures for lignin-containing cellulose nanofibrils obtained from various sources have been observed and described previously [16, 49, 50]. During TEMPO-mediated oxidation, lignin was oxidized and depolymerized to form small fragments of lignin. Due to its hydrophobic nature, lignin aggregated into spheres in order to minimize its contact surface with water [16]. The average diameter of the obtained LCNF 14 ± 5 nm nanofibrils was slightly smaller than the diameter of TOCNF nanofibrils. This was probably due to the different sources used to obtain TOCNF and LCNF. The morphology of $LCNF_1$ was less uniform than that of $LCNF_2$: lignin nanoparticles were located separately from cellulose nanofibrils and had a large size spread (14 ± 8 nm). Possibly, this morphology of $LCNF_1$ was due to structural changes in lignin upon mild hydrolysis of TMP_{pr} with dilute HCl. Longer $LCNF_2$ nanofibrils were uniformly coated with spherical lignin nanoparticles 10 ± 3 nm in size. However, aggregation, lack of aligned fibrils, and overlap of individual $LCNF_2$ nanofibrils made it difficult to accurately determine the length of nanofibrils using AFM. Spherical lignin nanoparticles on the surface of $LCNF_2$ nanofibrils could be associated with lignin redeposition [22]. It is worth noting that the lignin nanoparticles appeared to be attached to the $LCNF_2$ rather than separated from fibrils as for $LCNF_1$ specimens.

The resulting $LCNF_1$ and $LCNF_2$ films can be considered as nanocomposites of two nanosized biomaterials, cellulose and lignin. In order to study the effect of hydrophobic lignin on the wettability of films, the water contact angles (WCA) of TOCNF, $LCNF_1$, and $LCNF_2$ films were measured (Fig. 4g,h,i). TOCNF films were the most hydrophilic (WCA 39°) compared to $LCNF_1$ (WCA 75°) and $LCNF_2$ (WCA 82°) films. This behavior of TOCNF films can be explained not only by the difference in chemical composition (the absence of lignin), but by a decrease in surface roughness [51]. The mean surface roughness value (Ra) for TOCNF, estimated by AFM, was 20 times lower than Ra for $LCNF_1$ and more than 12 times lower than Ra for $LCNF_2$ (Table 2). Despite the higher Ra values for $LCNF_1$ and their higher lignin content, WCA films of $LCNF_1$ were lower than for $LCNF_2$ films. Apparently, larger lignin particles, located separately from cellulose nanofibrils, increased the surface roughness of $LCNF_1$ films (61 nm vs. 37 nm Ra for $LCNF_1$ films; Figs. 4e,f). However, a more uniform distribution of lignin nanoparticles over the surface of nanofibrils resulted in the greater hydrophobicity of $LCNF_2$ films compared to $LCNF_1$.

3.3. Optical and thermal properties of $LCNF_1$, $LCNF_2$ films

Translucent $LCNF_1$ and $LCNF_2$ films were obtained without cracks (Fig. 5). The $LCNF_2$ films were flexible (Figs. 5c,d) in contrast to the brittle $LCNF_1$ films (Figs. 5a,b). In the visible light region (400–800 nm), LCNF films showed optical transmission dependent on lignin content and film thickness. Comparison of the transmission spectra

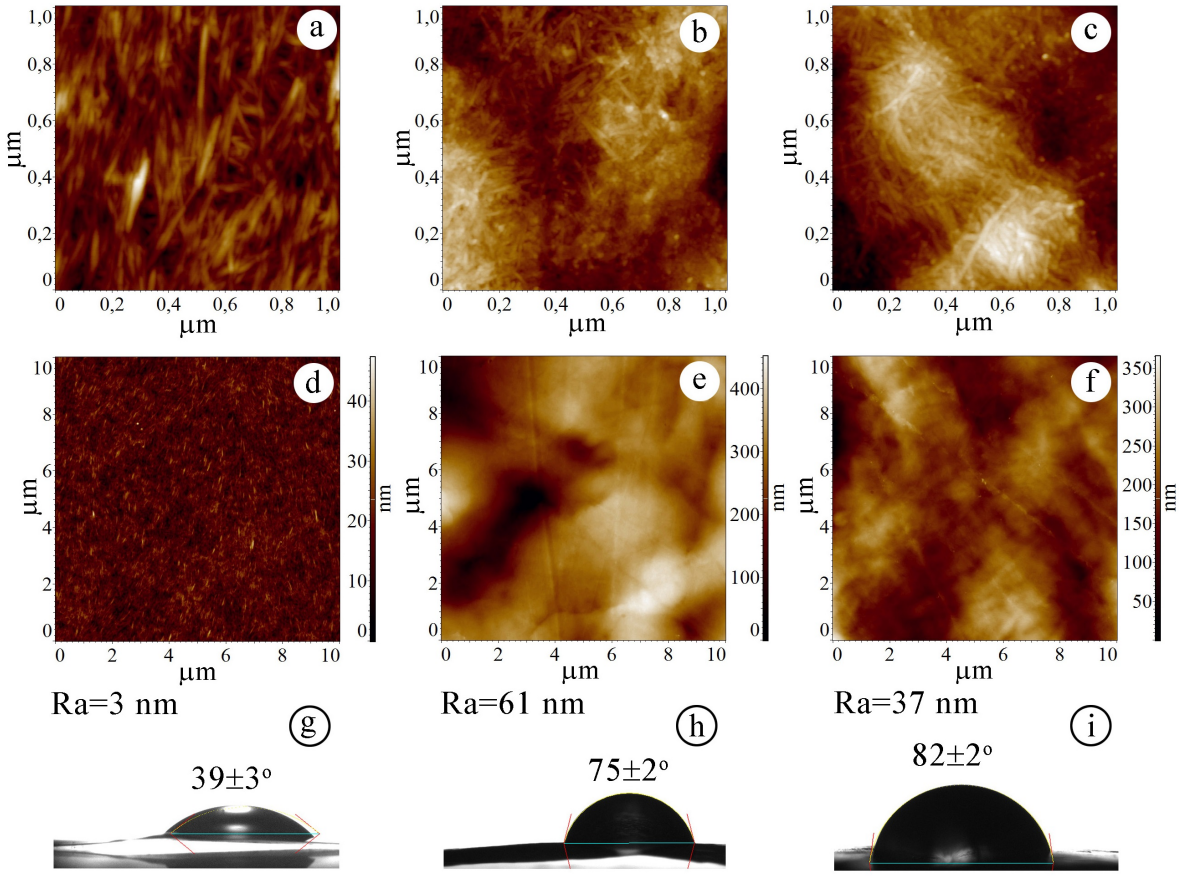

FIG. 4. AFM images of films: TOCNF (a,d), $LCNF_1$, (b,e), $LCNF_2$ (c,f). Images of a water droplet spreading over the films: TOCNF (g), $LCNF_1$, (h), $LCNF_2$ (i)

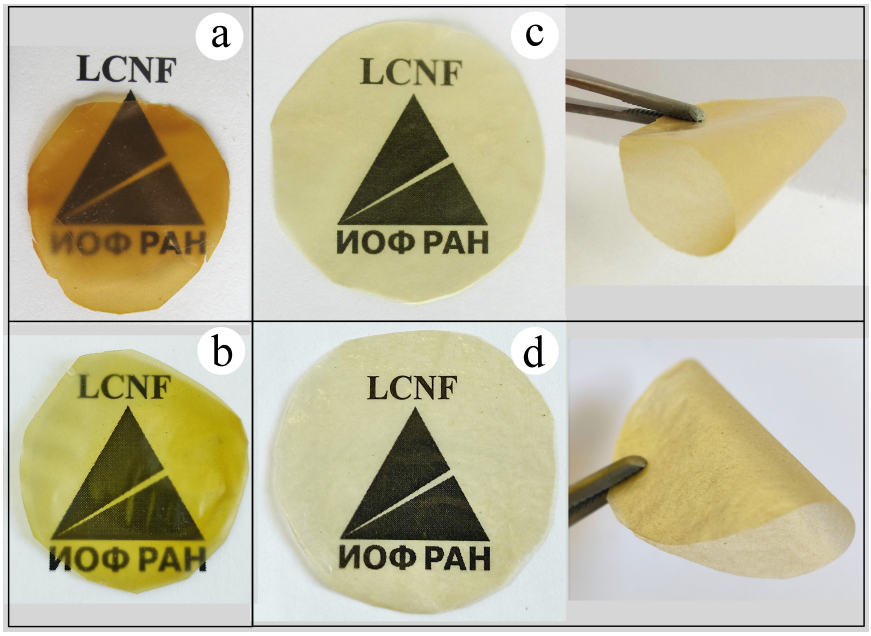

FIG. 5. Appearance of the films: $LCNF_1$ (a,b), $LCNF_2$ (c,d), obtained from suspensions of 2.2 wt.% and 1.1 wt.%, respectively. The logo is used with permission from Prokhorov General Physics Institute of the Russian Academy of Sciences

of LCNF films obtained from a dispersion with the same concentration showed that the lignin content makes the main contribution to the decrease in the transmission coefficient (Fig. 6, Table 3).

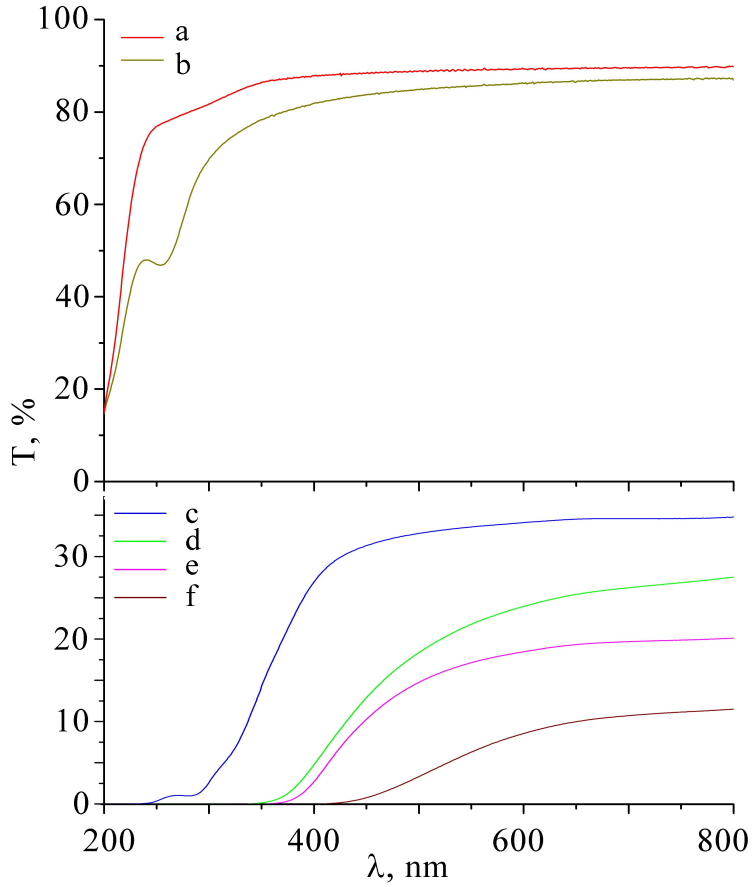

FIG. 6. Transmission spectra of the films: TOCNF (a,b), $LCNF_2$ (c,e), $LCNF_1$ (d,f), obtained from suspensions of 1.1 wt.% and 2.2 wt.%, respectively

TABLE 3. Optical properties of TOCNF, $LCNF_1$, $LCNF_2$ films

Sample	Suspension concentration, wt.%	Film thickness, μm	Transmittance (T), %			UV blocking ratio (R), %	
			600 nm	275 nm	350 nm	275 nm	350 nm
$LCNF_1$	1.1	20 ± 5	24.1	0	0	100	100
$LCNF_1$	2.2	40 ± 5	8.8	0	0	100	100
$LCNF_2$	1.1	$20\pm$	33.7	0.9	13.1	98.9	84.8
$LCNF_2$	2.2	40 ± 5	18.5	0	0.8	100	99.0
TOCNF	1.1	20 ± 5	89.4	80.0	86.2	0	0
TOCNF	2.2	35 ± 5	86.7	60.1	77.9	0	0

The $LCNF_1$ and $LCNF_2$ films showed strong absorption in both UVB (280–315 nm) and UVA (315–400 nm) compared to TOCNF films (Fig. 5). $LCNF_2$ films had a UV absorption band at 295–301 nm (Figs. 8b,c), due to the π–π interaction between lignin molecules [52]. The transmittance coefficients (T) and UV blocking ratio (R) of these films at 275 and 350 nm, respectively, were summarized in Table 3. The UV blocking ratios (R, %) were evaluated using equation (1) [53]:

$$R = \frac{(T_0 - T) \cdot 100}{T_0}, \tag{1}$$

where the transmittance coefficients of TOCNF and LCNF films were defined as T_0 and T, respectively.

The $LCNF_1$ films exhibited a pronounced UV blocking property in the wavelength range below 375 nm (Fig. 5c,e). $LCNF_2$ films showed high UV blocking effect in both UVB (R = 99%–100%) and UVA (R = 84.8%–99.0%) with a decrease in transmission at 600 nm (T = 33.7–18.5%), depending on the film thickness (Table 3).

Thermal stability of LCNF and TOCNF films as well as TMP_{pr} was evaluated by thermogravimetric analysis (TG) under synthetic air flow (Fig. 7). The initial weight losses at 150°C for TMP_{pr}, TOCNF films, $LCNF_1$, and $LCNF_2$ were 7.9%, 7.0%, 5.9%, and 6.7%, respectively; and they were attributed to the adsorbed water evaporation. The initial and the final decomposition temperatures (T_{onset} and T_{endset}) were defined as the temperatures at which the sample weight losses became more apparent, and at which the weight losses stopped, respectively.

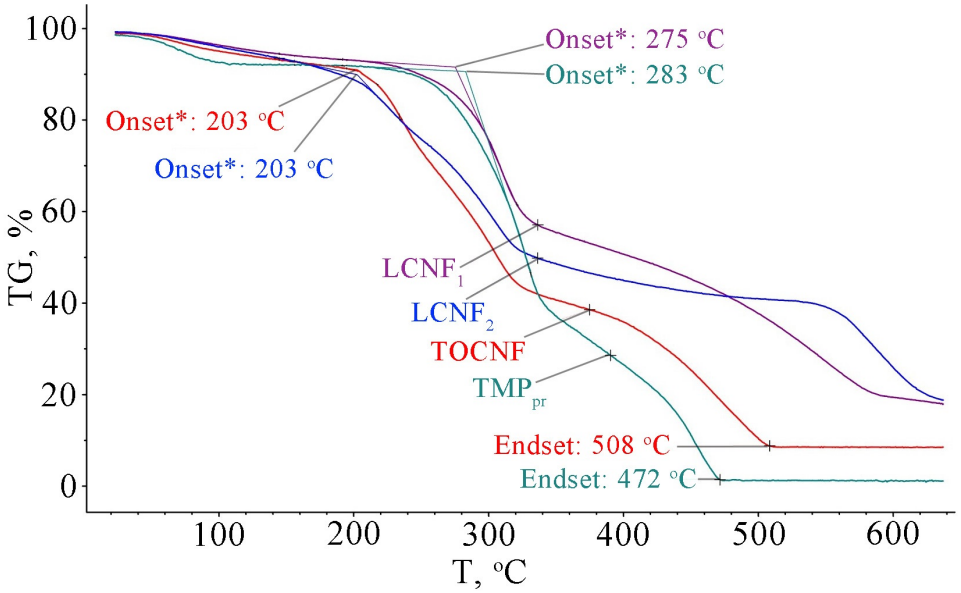

FIG. 7. TG curves for TMP_{pr} and films: TOCNF, $LCNF_1$, $LCNF_2$

The initial weight losses at 150°C for TMP_{pr}, TOCNF films, $LCNF_1$, and $LCNF_2$ were 7.9%, 7.0%, 5.9%, and 6.7%, respectively; and they were attributed to the adsorbed water evaporation. The initial and final decomposition temperatures (T_{onset} and T_{endset}) were defined as the temperatures at which the sample weight losses became more apparent, and at which the weight losses stopped, respectively. T_{onset} for TMP_{pr}, (283°C) and T_{onset} for $LCNF_1$ (275°C) differed insignificantly by 8°C due to the high content of lignin in them, Table 1. Lignin, composed of phenyl-propane units interconnecting via various ether and carbon-carbon bonds, is more thermally stable then cellulose and hemicelluloses [45]. The decrease of T_{onset} of $LCNF_1$ was probably associated with an increase in the heat exchange rate due to the surface area increase and decrease in the particle size to nanoscale. The decomposition proceeds of TOCNF and $LCNF_2$ films occurred at lower temperatures comparing to $LCNF_1$ film and TMP_{pr}, Fig. 7. The decrease in the TEMPO oxidation of lignocellulosic biomass thermal destruction temperature due to the influence of carboxylate groups has been thoroughly studied Rohaizu and Wanrosli [45]. We believe that the lower temperatures (T_{onset}) for thermal decomposition (203°C) of TOCNF and $LCNF_2$ films are due to the higher content of carboxyl groups, Table 1. The TG curves of all samples showed three stages of degradation with overlapping stages of degradation of various components. The first stage was associated with the loss of moisture. The second stage of decomposition was associated with dehydration, depolymerization of hemicelluloses and cellulose. The third stage of sample decomposition can be explained by the oxidation of residual carbon [8] and the degradation of the complex structure of lignin [22]. For TMP_{pr} and TOCNF film, the final decomposition temperatures T_{endset} were determined to be 579°C and 508°C, respectively. The increased value of T_{endset} TMP_{pr} was associated with the high thermal stability of the aromatic chain of lignin. For $LCNF_1$ and $LCNF_2$ films, the final decomposition temperature was not determined; the residue at 650°C was 17.5% and 18.1%, respectively, which significantly exceeds the residue for TMP_{pr} (1.1%). This indicates that the incorporation of carboxylate functional groups into $LCNF_1$ and $LCNF_2$ as a result of TEMPO oxidation had a flame retardant effect. The high content of lignin at a low content of carboxyl groups led to an increase in the thermal stability of $LCNF_1$ films. The high content of carboxyl groups with a simultaneous decrease in the content of lignin contributed to a decrease T_{onset} of $LCNF_2$ films to 203°C. The $LCNF_1$ and $LCNF_2$ films exhibited flame retardant properties.

4. Conclusions

We developed the efficient process for the isolation of 14 ± 5 nm diameter lignin-containing cellulose nanofibrils from TMP using TEMPO oxidation followed by sonication. The 23.8 wt% lignin content in $LCNF_1$, isolated with the use of dilute HCl prehydrolysis and a low dose of NaClO (5 mmol/g), was much higher than the same ingredient content reported in any previously published studies. The lignin content decreased to 14.1% in $LCNF_2$ with the increase of NaClO load to 10 mmol/g, while the content of carboxyl groups in $LCNF_2$ increased to 1.24 mmol/g (vs. 0.70 mmol/g for $LCNF_1$).

Thin (20–40 μm), translucent, and flexible $LCNF_2$ films with a uniform distribution of 10 ± 3 nm spherical lignin nanoparticles and more brittle $LCNF_1$ films with less uniform distribution of larger (14 ± 8 nm) lignin nanoparticles were obtained by a solution casting technique. LCNF films showed excellent UV-blocking ability in a wide spectrum range from 200 to 375 nm, and much less hydrophilicity (WCA = 75–82°) compared to TOCNF films (WCA = 39°). The thermal stability of LCNF films increased with an increase in the lignin content and a decrease in the content of carboxyl groups up to 275 °C compared to 203 °C TOCNF films.

Overall, LCNF can be considered as nanocomposite. The presence of nanolignin on the surface of LCNF resulted in a UV blocking effect, an increase in thermal stability, and increase of hydrophobicity of obtained films. The developed process has provided LCNFs with high yield and superior properties for making the packaging materials and/or biopolymer composites.

References

[1] Ahankari S.S., Subhedar A.R., Bhadauria S.S., Dufresne A. Nanocellulose in food packaging: a review. *Carbohyd. Polym.*, 2020, **255**, P. 117479.

[2] Liu Z., Zhang S., He B., et al. Synthesis of cellulose aerogels as promising carriers for drug delivery: a review. *Cellulose*, 2021, **28**, P. 2697–2714.

[3] De Amorim J.D.P., de Souza K.C., Duarte C.R., et al. Plant and bacterial nanocellulose: production, properties and applications in medicine, food, cosmetics, electronics and engineering: a review. *Environ. Chem. Lett.*, 202, **18**, P. 851–869.

[4] Fedorov P.P., Luginina A.A., Kuznetsov S.V., et al. Composite up-conversion luminescent films containing a nanocellulose and SrF_2:Ho particle. *Cellulose*, 2019, **26**, P. 2403–2423.

[5] De France K., Zeng Z., Wu T., Nyström G. Functional Materials from Nanocellulose: Utilizing Structure-Property Relationships in Bottom-Up Fabrication. *Advanced Materials*, 2021, **33**(28), P. 2000657.

[6] Dias O.A.T., Konar S., Leão A.L., et al. Current State of Applications of Nanocellulose in Flexible Energy and Electronic Devices. *Frontiers in Chemistry*, 2020, **8**, P. 420.

[7] Nie S., Hao N., Zhang K., et al. Cellulose nanofibrils-based thermally conductive composites for flexible electronics: a mini review. *Cellulose*, 2020, **27**, P. 4173–4187.

[8] Fedorov P.P., Luginina A.A., Kuznetsov S.V., et al. Hydrophobic up-conversion carboxylated nanocellulose/fluoride phosphor composite films modified with alkyl ketene dimer. *Carbohyd. Polym.*, 2020, **250**, P. 116866.

[9] Luginina A.A., Kuznetsov S.V., Ivanov, V.K. et al. Laser damage threshold of hydrophobic up-conversion carboxylated nanocellulose/SrF_2:Ho composite films functionalized with 3-aminopropyltriethoxysilane. *Cellulose*, 2021, **28**, P. 10841–10862.

[10] Guan Q.F., Yang H.B., Han Z.M., et al. An all-natural bioinspired structural material for plastic replacement. *Nat. Commun.*, 2020, **11**(1), P. 1–7.

[11] Turbak A.F., Snyder F.W., Sandberg K.R. Microfibrillated cellulose, a new cellulose product: properties, uses and commercial potential. *J. Appl. Polym. Sci.*, *Appl. Polym. Symp.*, 1983, **37**, P. 815–827.

[12] Herrick F.W., Casebier R.L., Hamilton J.K., Sandberg K.R. Microfibrillated cellulose: morphology and accessibility. *J. Appl. Polym. Sci.*, Appl. Polym. Symp., 1983, **37**, P. 797–813.

[13] Klemm D., Kramer F., Moritz S., et al. Nanocelluloses: a new family of nature-based materials. *Angew. Chem. Int. Ed.*, 2011, **50**, P. 5438–5466.

[14] Klemm D., Cranston E., Fischer D., et al. Nanocellulose as a natural source for groundbreaking applications in materials science: today's state. *Mater. Today*, 2018, **21**, P. 720–748.

[15] Park C.W, Han S.Y, Namgung H.W, et al. Preparation and characterization of cellulose nanofibrils with varying chemical compositions. *BioResources*, 2017, **12**(3), P. 5031–5044.

[16] Nader S., Brosse N., Khadraoui M., et al. A low-cost environmentally friendly approach to isolate lignin containing micro and nanofibrillated cellulose from Eucalyptus globulus bark by steam explosion. *Cellulose*, 2022, **29**, P. 5593–5607.

[17] Oliaei E., Lindén P.A., Wu Q. et al. Microfibrillated lignocellulose (MFLC) and nanopaper films from unbleached kraft softwood pulp. *Cellulose*, 2020, **27**, P. 2325–2341.

[18] Diop C.I.K., Tajvidi M., Bilodeau M. A., et al. Evaluation of the incorporation of lignocellulose nanofibrils as sustainable adhesive replacement in medium density fiberboards. *Industrial Crops and Products*, 2017, **109**, P. 27–36.

[19] Khadraoui M., Khiari R., Bergaoui L., Mauret E. Production of lignin-containing cellulose nanofibrils by the combination of different mechanical processes. *Industrial Crops and Products*, 2022, **183**, P. 114991.

[20] Espinosa E., Domínguez-Robles J., Sánchez R., et al. The effect of pre-treatment on the production of lignocellulosic nanofibers and their application as a reinforcing agent in paper. *Cellulose*, 2017, **24**, P. 2605–2618.

[21] Terrett O.M, Lyczakowski J.J., et al. Molecular architecture of softwood revealed by solid-state NMR. *Nat. Commun.*, 2019, **10**, P. 4978.

[22] Liao J., Latif N.H.A., Trache D., et al. Current advancement on the isolation, characterization and application of lignin. *Int. J. Biol. Macromol.*, 2020, **162**, P. 985–1024.

[23] Solala I., Iglesias M.C., Peresin M.S. On the potential of lignin-containing cellulose nanofibrils (LCNFs): a review on properties and applications. *Cellulose*, 2020, **27**, P. 1853–1877.

[24] Sadeghifar H., Venditti R., et al. Cellulose-lignin biodegradable and flexible UV protection film. *ACS Sustain Chem. Eng.*, 2017, **5**, P. 625–631.

[25] Farooq M., Zou T., Riviere G., et al. Strong ductile and waterproof cellulose nanofibril composite films with colloidal lignin particles. *Biomacromolecules*, 2018, **20**, P. 693–704.

[26] Huang C., Dong H., Zhang Z. et al. Procuring the nano-scale lignin in prehydrolyzate as ingredient to prepare cellulose nanofibril composite film with multiple functions. *Cellulose*, 2020, **27**, P. 9355–9370.

[27] Chen Y., Fan D., Han Y. et al. Effect of high residual lignin on the properties of cellulose nanofibrils/films. *Cellulose*, 2018, **25**, P. 6421–6431.

[28] Lê H.Q., Dimic-Misic K., Johansson L., et al. Effect of lignin on the morphology and rheological properties of nanofibrillated cellulose produced from γ-valerolactone/water fractionation process. *Cellulose*, 2018, **25**, P. 179–194.

[29] Liu K., Du H., Zheng T., et al. Lignin-containing cellulose nanomaterials: preparation and applications. *Green. Chem.*, 2021, **23**(24), P. 9723–9746.

[30] Ferrer A., Hoeger I.C., et al. Reinforcement of polypropylene with lignocellulose nanofibrils and compatibilization with biobased polymers. *J. Appl. Polym. Sci.*, 2016, **133**, P. 43854.

[31] Visanko M., Sirviö J.A., Piltonen P., et al. Castor oil-based biopolyurethane reinforced with wood microfibers derived from mechanical pulp. *Cellulose*, 2017, **24**, P. 2531–2543.

[32] Herzele S., Veigel S., Liebner F., et al. Reinforcement of polycaprolactone with microfibrillated lignocellulose. *Ind. Crops. Prod.*, 2016, **93**, P. 302–308.

[33] Ballner D., Herzele S., Keckes J., et al. Lignocellulose nanofiber-reinforced polystyrene produced from composite microspheres obtained in suspension polymerization shows superior mechanical performance. *ACS Appl. Mater. Interfaces*, 2016, **8**, P. 13520–13525.
[34] Isogai A., Kato Y., Preparation of polyuronic acid from cellulose by TEMPO-mediated oxidation. *Cellulose*, 1998, **5**, P. 153–164.
[35] Isogai T., Saito T., Isogai A. Wood cellulose nanofibrils prepared by TEMPO electro-mediated oxidatin. *Cellulose*, 2011, **18**, P. 421–431.
[36] Saito T., Kimura S., et al. Cellulose nanofibers prepared by TEMPO-mediated oxidation of native cellulose. *Biomacromolecules*, 2007, **8**, P. 2485–2491.
[37] Luginina A.A., Kuznetsov S.V., Ivanov V.K., et al. Dispersibility of freeze-drying unmodified and modified TEMPO-oxidized cellulose nanofibrils in organic solvents. *Nanosystems: Phys., Chem., Math.*, 2021, **12**(6), P. 763–772.
[38] Jiang F., Han S., Hsieh Y.L. Controlled defibrillation of rice straw cellulose and selfassembly of cellulose nanofibrils into highly crystalline fibrous materials. *RSC Advances*, 2013, **3**(30), P. 12366–12375.
[39] Chen Y.W., Lee H.V., Juan J.C., Phang S.M. Production of new cellulose nanomaterial from red algae marine biomass Gelidium elegans. *Carbohyd. Polym.*, 2016, **151**, P. 1210–1219.
[40] Sluiter J.B., Ruiz R.O., Scarlata C.J., Sluiter A.D., Wolfrum E.J. Compositional Analysis of Lignocellulosic Feedstocks. 1. Review and Description of Methods. *Agric. Food Chem.*, 2010, **58**(16), P. 9043–9053.
[41] Nikitin V.M., Obolenskaya A.V., Schegolev V.P. *Chemistry of wood and cellulose*. M.: Lesnay promyshlennost, 1978, 368 p. (in Russian)
[42] Brännvall E., Aulin C. CNFs from softwood pulp fibers containing hemicellulose and lignin. *Cellulose*, 2022, **29**, P. 4961–4976.
[43] Bikales N.M., Segal L. *Cellulose and cellulose derivatives*, Part 2, M.: Mir, 1974, 510 p. (in Russian)
[44] Zhao C., Zhang H., Li, Z. et al. Further understanding the influence of fiber surface and internal charges on the interfiber bonding capability and resulting paper strength. *Cellulose*, 2017, **24**, P. 2977–2986.
[45] Rohaizu R., Wanrosli W.D. Sono-assisted TEMPO oxidation of oil palm lignocellulosic biomass for isolation of nanocrystalline cellulose. *Ultrason. Sonochem.*, 2017, **34**, P. 631–639.
[46] Deepa B., Abraham E., Cordeiro N. et al. Utilization of various lignocellulosic biomass for the production of nanocellulose: a comparative study. *Cellulose*, 2015, **22**, P. 1075–1090.
[47] Yao J., Odelius K., Hakkarainen M. Microwave Hydrophobized Lignin with Antioxidant Activity for Fused Filament Fabrication. *ACS Appl. Polym. Mater.*, 2021, **3**(7), P. 3538–3548.
[48] Sun X.F., Xu F., Sun R.C., et al. Characteristics of degraded cellulose obtained from steamexploded wheat straw. *Carbohydr Res.*, 2005, **340**, P. 97–106.
[49] Yang M., Zhang X., Guan S., et al. Preparation of lignin containing cellulose nanofibers and its application in PVA nanocomposite films. *Int. J. Biol. Macromol.*, 2020, **158**, P. 1259–1267.
[50] Jiang Y., Wang Z., Liu X., et al. Highly Transparent, UV-Shielding, and Water-Resistant Lignocellulose Nanopaper from Agro-Industrial Waste for Green Optoelectronics. *ACS Sustain. Chem. Eng.*, 2020, **8**(47), P. 17508–17519.
[51] Wenzel R.N. Resistance of Solid Surfaces to Wetting by Water. *Ind. Eng. Chem.*, 1936, **28**(8), P. 988–994.
[52] Fu H., Li Y., Wang B., et al. Structural change and redispersion characteristic of dried lignin-containing cellulose nanofibril and its reinforcement in PVA nanocomposite film. *Cellulose*, 2021, **28**, P. 7749–7764.
[53] Li Y., Zou Y., Hou Y. Fabrication and UV-blocking property of nano-ZnO assembled cotton fibers via a two-step hydrothermal method. *Cellulose*, 2011, **18**, P. 1643–1649.

Submitted 7 September 2022; accepted 10 November 2022

Information about the authors:

Anna A. Luginina – Prokhorov General Physics Institute of the Russian Academy of Sciences, 38 Vavilov str., Moscow 119991, Russia; ORCID 0000-0002-6564-5729; ana@lst.gpi.ru

Sergey V. Kuznetsov – Prokhorov General Physics Institute of the Russian Academy of Sciences, 38 Vavilov str., Moscow 119991, Russia; ORCID 0000-0002-7669-1106; kouznetzovsv@gmail.com

Alexander A. Alexandrov – Prokhorov General Physics Institute of the Russian Academy of Sciences, 38 Vavilov str., Moscow 119991, Russia; ORCID 0000-0001-7874-7284; alexandrov1996@yandex.ru

Radmir V. Gainutdinov – Shubnikov Institute of Crystallography of Federal Scientific Research Centre Crystallography and Photonics of Russian Academy of Sciences, 59 Leninsky Pr., Moscow, 119333, Russia; ORCID 0000-0002-5384-4026; rgaynutdinov@gmail.com

Dmitrii I. Petukhov –Lomonosov Moscow State University, Chemical department, 1 Leninskie Gory, Moscow, 119991, Russia; ORCID 0000-0002-0956-5820; di.petukhov@gmail.com

Valery V. Voronov – Prokhorov General Physics Institute of the Russian Academy of Sciences, 38 Vavilov str., Moscow 119991, Russia; ORCID 0000-0001-5029-8560; voronov@lst.gpi.ru

Elena V. Chernova – Prokhorov General Physics Institute of the Russian Academy of Sciences, 38 Vavilov str., Moscow 119991, Russia; ORCID 0000-0001-7401-5019; e-chernova@yandex.ru

Pavel P. Fedorov – Prokhorov General Physics Institute of the Russian Academy of Sciences, 38 Vavilov str., Moscow 119991, Russia; ORCID 0000-0002-2918-3926; ppfedorov@yandex.ru

Conflict of interest: the authors declare no conflict of interest.